Self-assembling and ordering of Ge/Si(111) quantum dots: scanning microscopy probe studies

2002 J. Phys.: Condens. Matter 14 8353

(http://iopscience.iop.org/0953-8984/14/35/308)

INSTITUTE OF PHYSICS PUBLISHING JOURNAL OF PHYSICS: CONDENSED MATTER

J. Phys.: Condens. Matter **14** (2002) 8353–8378 PII: S0953-8984(02)34333-9

Self-assembling and ordering of Ge/Si(111) quantum dots: scanning microscopy probe studies

Nunzio Motta[1]

INFM–Dipartimento di Fisica Università di Roma TRE, Via della Vasca Navale 84, 00146 Roma, Italy

E-mail: motta@fis.uniroma3.it

Received 27 February 2002, in final form 23 May 2002
Published 22 August 2002
Online at stacks.iop.org/JPhysCM/14/8353

Abstract

In order to exploit the unique electronic properties of semiconductor quantum dots (QDs) in novel quantum effect devices, the lateral dimensions of these structures have to be reduced to the order of tens of nanometres, which is the range of the de Broglie wavelength of electrons inside these materials. Moreover, millions of QDs should be packed in an orderly fashion in dense arrays to achieve the necessary active volume. So far, the most promising quantum structures have been fabricated using techniques based on direct crystal growth. This process has become very important due to its potential for creating damage-free and coherent nanocrystals. New scanning microscopy probes, such as scanning tunnelling microscopy and atomic force microscopy, are actually the most important analytical tools for checking the properties of these nanostructures. In the present paper we will review some of the results recently obtained on the Ge/Si system thanks to these techniques. Ge/Si is really appealing for future applications, in view of the integration of nanostructures with the present microelectronic technologies, but it is also at the origin of many general studies regarding atomic diffusion, intermixing, and island shape stabilization. The origin of the islands, their size and shape evolution, and the intermixing at the interface will be analysed starting from SPM data. The ordering of QDs on naturally or artificially nanostructured surfaces is one of the most recent objectives in Ge/Si research. For example, terraces created from the step bunching process on the Si(111) surface could be a way of controlling the spacing of the islands. Other possibilities are now opened by the increasing precision of electron-beam lithography and by new focused-ion-beam machines. These aspects, along with problems and drawbacks of self-assembling technology, will also be discussed.

(Some figures in this article are in colour only in the electronic version)

[1] Former address: INFM–Dipartimento di Fisica, Università di Roma Tor Vergata, Via della Ricerca Scientifica 1, 00133 Roma, Italy.

1. Introduction

A semiconductor quantum dot (QD) is the ultimate quantum confined structure. Its unique electronic properties rely on the δ-function-like energy dependence of the density of states due to the quantum confinement of carriers in all three dimensions. However, in order to exploit the electronic properties in new quantum effect devices, the lateral dimensions of the structures have to be in the range of, or smaller than, the de Broglie wavelength of the electrons inside the material.

Advances in crystal growth techniques such as MBE and metal–organic vapour phase epitaxy (MOVPE) have made it possible to precisely fabricate two-dimensional layered semiconductors, i.e. heterojunctions, quantum wells, and superlattices, on an atomic scale. Further reduction of the dimensionality of semiconductors in one-dimensional quantum wires and zero-dimensional QDs is achieved thanks to heteroepitaxy, by exploiting the lattice mismatch between different semiconductors. Self-assembly of islands in heteroepitaxial growth originates from the strain caused by the lattice parameter difference between the epilayer and the substrate. The growth of a heteroepitaxial wetting layer is possible thanks to the tetragonal deformation of the epilayer, in the presence of a 'coherent strain', up to a certain limit (3–5 ML for Ge–Si and at 1.5–2 ML for InAs/GaAs). Beyond this limit, the energy of the system can be lowered by the formation of 3D islands. These 'QDs' are really perfect 'nanocrystals', which are, within certain limits, undislocated and defect free. In this work we will concentrate on Ge–Si QDs. The interest in these structures has rapidly increased in the last few years, because they represent one possible way to create optoelectronic devices directly on Si, which is optically inactive. The indirect band gap of Si is not suited for optoelectronics, but it is possible to 'engineer' the band gap by creating structures smaller than the electronic wavelength. In this case the electrons are confined and the energy levels are those of a 'particle in a box'. A large increase in photoluminescence has been observed for these structures. Ge is the most suited element for obtaining this result because it has the same crystal structure, and a lattice parameter smaller than that of Si by 4%. Due to this lattice mismatch, the epitaxial growth of Ge on Si gives rise to nanoislands with dimensions ranging from 80 up to 300 nm. The island size is a function of the intermixing between Ge and Si, which in turn depends on the growth temperature. The term 'QDs', in principle, should be used only for those structures smaller than the de Broglie wavelength (about 50 nm in GaAs), but it is common practice to extend this term to larger nanocrystals, originating from heteroepitaxial growth.

Such small structures, which must fulfil the stringent requirement of very high uniformity in shape and dimensions, need special analytical tools for checking in order to guarantee a perfect integration with circuitry fabrication. Damage-free structures and coherent nanocrystals are required for applications. It is well known, in fact, that defects are traps for the electrons and can substantially modify the expected characteristics of a device. Structural control of these QDs can easily be achieved now thanks to the new scanning microscopy probes (SPM), such as scanning tunnelling microscopy and atomic force microscopy (AFM) [1–3]. Other techniques are also used to check *in situ* the epitaxial growth (RHEED), and for the control of QD composition (EXAFS), but SPM gives by far the most useful and direct information. Spectacular three-dimensional images are obtained, from the reconstructions on the island surfaces up to the direct visualization of the epitaxial growth. In the case of semiconductor epitaxy the possibility of having microscopic images in real space, rather than in reciprocal space, helps very much in understanding the growth process of the nanostructures. In fact, hardly any experimental paper dealing with the epitaxial growth of QDs can be published without an SPM image of the grown structures. Among the standard techniques of microscopy such as SEM and TEM, only the latter can give complementary

information to SPM, since it visualizes the bulk of the structure, evidencing the growth mode, crystal stress, dislocations, and bulk defects which are not visible at the surface. All these data are needed to check the quality of the epitaxy, but the sample must be destroyed and the specimen preparation is quite lengthy and complex. Therefore AFM is preferred whenever a quick check of the sample is needed. The STM is used to visualize *in situ* the grown nanostructures, both during and after growth, before any contaminant can destroy the surface. TEM is usually applied only to selected samples to visualize their internal structure.

Normally an SPM is used to image a surface without causing it damage or introducing modifications. However, in the early 1990s scientists found that the SPM can be used also to modify the surface deliberately, for example by manipulating single atoms on surfaces, thus allowing nanostructures to be built in a 'bottom-up' fashion. Recent experiments aim at controlling the nanostructures' nucleation site by using the STM or AFM tip as a tool to modify the surface at predetermined locations (for example by producing holes, by oxidizing the surface by the AFM tip in air, or by depositing some material through voltage pulses from the STM tip) [4, 5]. We will not deal with this kind of experiment since we are interested in the self-assembling properties of the Ge/Si system. It should be noted, moreover, that the self-assembling of QDs during epitaxial growth is by far the most convenient way of creating nanostructures. No other way is so fast and well suited for industrial processes.

We will start by giving some details about the different techniques used to obtain self-assembled QDs. After that we will tackle the problem of heteroepitaxy, which involves a strain in the epitaxial layer. We will describe the different growth modes, as a consequence of increasing lattice mismatch and epitaxial strain. The nucleation and the evolution of coherent islands will be illustrated in different cases, notably for Ge/Si(111). Self-ordering of islands on stepped surfaces will also be taken into account. Finally we will consider the problem of the stabilization of the islands' shape and dimension.

2. Growth techniques

Three different epitaxial techniques are available today for the production of self-assembled QDs: chemical vapour deposition (CVD), molecular-beam epitaxy (MBE), and physical vapour deposition (PVD). While the CVD is the best one for industrial production, due to its high growth rate, the other two are more suited for conducting growth studies.

2.1. Chemical vapour deposition

CVD uses special hydrogen-based molecules for the transport of the atomic species needed for epitaxy. For Ge–Si epitaxy GeH_4 (germane) and SiH_4 (silane) are typically used, at pressures ranging from some millibar (high-pressure CVD) to 10^{-5} millibars (low-pressure CVD). A reaction occurs close to the surface, which is kept at high temperature (400–700 °C); the molecular cracking leaves the epitaxial species attached to the surface bonds, while the rest of the molecule is evacuated by the pumping system. Growth rates in the range 0.1–100 nm min^{-1} are possible with this technique.

2.2. Molecular-beam epitaxy

MBE is used for very clean growth when a limited amount of deposited material is necessary. It is very useful indeed for studies on epitaxy, because through the reflecting high-energy electron diffraction (RHEED) technique it is possible to follow the growth layer after layer and detect the formation of 3D structures. An MBE apparatus consists of a UHV chamber, with several

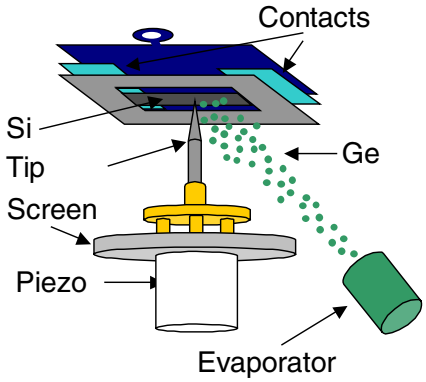

Figure 1. The STM stage, capable of simultaneous evaporation and STM imaging.

solid-state sources (Knudsen cells) directed to the substrate, which usually can rotate to make the epitaxy more homogeneous. Cold shields guarantee a very low level of contamination. Starting vacuum levels are usually in the 10^{-11} mbar range, while, during the growth, pressures of 10^{-9} mbar can be attained. Typical growth rates are in the range 0.01–20 nm min^{-1}.

2.3. Physical vapour deposition

PVD is a simplified version of MBE, without RHEED control and cold shields. So it cannot be guaranteed that the contamination level is as low as in the case of MBE. However, it is easier to set up, and can be combined with other techniques such as STM or AFM. The sample is kept at the desired temperature by direct heating (the Joule effect through it) or by an appropriate resistor put on the back; the epitaxial material is evaporated from electron-bombarded or resistively heated crucibles. The typical growth rates range from 0.001 up to 1 nm min^{-1}. These rates are very low for thick layers and industrial production, but they are tailored to optimize STM growth studies.

2.4. The experimental set-up for imaging the MBE growth

The first apparatus capable of simultaneous MBE and STM imaging at high temperature was developed by Voigtlaender in 1993 [3], who studied extensively Si homoepitaxy, and the growth of Ge on Si(111) and Si(100). The microscope is an inverse Besocke model, with special screens for the piezoresistors, which allow minimization of thermal drift and contamination.

We have used a similar instrument, now commercially available, to study Ge growth on Si(111). In figure 1 a diagram of the STM stage is provided, showing the sample holder (with contacts for sample heating) and evaporation source.

3. Ge–Si heteroepitaxy

The word ‘epitaxy’ (from the Greek words $\varepsilon\pi\iota$ (on top) and $\tau\alpha\xi\iota\sigma$ (to order)) indicates a growth mode in which the atoms attach to an existing crystalline surface by forming layers with the same order as the original matrix. We define ‘heteroepitaxy’, an epitaxial growth realized by depositing an atomic species on a substrate with different composition.

The forces that act between the substrate and the deposited layer give rise to three kinds of growth mode: layer-by-layer (Frank–Van der Merwe), island formation on the bare substrate

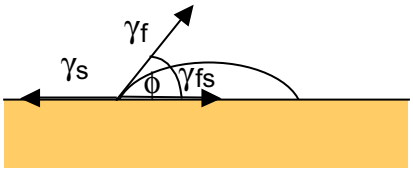

Figure 2. Forces at the film–substrate interface.

(Volmer–Weber), and a mix of the two: layer by layer up to a critical thickness and island formation above (Stranski–Krastanov). The basic equation that governs the growth mode is the Young–Dupré equation, which can be written as

$$\gamma_s = \gamma_f \cos\phi + \gamma_{fs} \tag{3.1}$$

where γ_s is the surface free energy of the substrate and γ_f and γ_{fs} are the surface and interface energies of the film (figure 2). From a thermodynamic point of view the three growth modes can be derived from the sign of $\Delta\gamma = \gamma_f + \gamma_{fs} - \gamma_s$. In fact, for layer-by-layer growth, because the surface formation energy γ_s is larger than that of the islands, $\Delta\gamma < 0$ and $\cos\phi = 1$ (this is the case of lattice-matched systems; for example, Si on Si). Alternatively, if γ_s is smaller than $\gamma_f + \gamma_{fs}$, this means that $\Delta\gamma > 0$ and for (2.1) to hold we must have $\cos\phi < 0$; this means that 3D clusters nucleate on the substrate. This growth mode is typical of large-lattice-mismatch systems, for example Ag on GaAs. If it happens that $\Delta\gamma$ is negative for the first few monolayers and then changes sign at a critical layer thickness, the growth mode changes from 2D to 3D (Stranski–Krastanov). This mode is typical of small-lattice-mismatch systems, for example Ge on Si or InAs/GaAs. Ge/Si could be regarded as a model SK system, because both species belong to the IV group, their bond being always covalent, without any ionic character. So the enthalpy at the Ge–Si interface depends essentially on the elastic energy connected to the bond deformation, and the calculation is particularly simple. However, the mixing of the two species is greatly favoured notably at high temperature, and this fact must be taken into account in the evaluation of the free energy, requiring much more complex calculations. This intermixing is also a serious limitation on the growth of small-sized QDs, because it lowers the real lattice mismatch, giving rise to large islands. All these points will be extensively discussed in the following subsections.

3.1. Growth of the wetting layer

Ge–Si is a prototype of small-lattice-mismatch systems, and the growth of its wetting layer on the Si(111) surface has been followed by STM by several authors [6–8]. At $T = 350\,^{\circ}\mathrm{C}$ and at a deposition rate of a few tenths of monolayers per minute it is possible to obtain a 'movie' (figure 3(a)) showing that the islands nucleate as perfect triangles, and coalesce to give a complete layer [8].

When atoms join to form a 2D island, the cohesive energy between the atoms acts to protect the island from dissociation: the free energy of the island is negative. Atoms at the edges of the island necessarily have fewer neighbours, and therefore more unsaturated bonds, which add a positive destabilizing 'boundary free energy' to the total free energy of the 2D island; the boundary free energy is the 1D analogue of the surface free energy. In order to nucleate an island, enough atoms must meet to make the total island free energy negative, because initially the boundary free energy dominates and the total free energy becomes more positive as atoms are added.

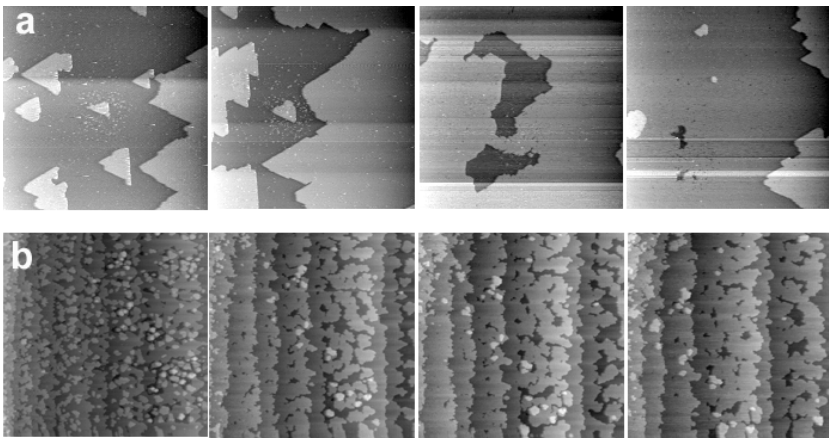

Figure 3. Ge/Si(111): growth of the wetting layer at $T = 400\,^{\circ}$C: (a) on a step-bunched surface with large terraces, low flux (0.02 ML min^{-1}); 0.3×0.3 μm^2 STM images; (b) on a regular surface with small steps, higher flux (0.15 ML min^{-1}); 1×1 μm^2 STM images. Full movies are available at the www.fisica.uniroma2.it/infm/nanolab Web site.

As islands continue to grow, specific island morphologies or shapes develop. One class of shapes—including squares, triangles and hexagons, and the corresponding 3D structures—is compact, with relatively straight and equiaxed island edges. Another class is fractal-like, having rough island edges or highly anisotropic shapes. Typically, growth at lower temperatures leads to less compact islands: the compactness of an island is mainly dominated by how fast an adatom diffuses along the island edges and crosses corners where two edges meet. In the movie it is interesting to see that subsequent layers form, starting from islands of more rounded shapes, with fractal-like borders (figure 3(b)). The evolution of the wetting layer in Ge/Si(111) has been also discussed recently by my group [6], and it is shown in figure 4, starting at 0.65 ML and going up to 2 ML where the percolation threshold is attained.

The process of coalescence has been modelled by assuming that the clusters are uniformly and randomly distributed over the surface [9] and that the nucleation rate of all clusters is δ-like [10]. For triangular islands the dependence of the total perimeter per unit area P of the islands on the fraction of covered surface S is given by

$$P(S) = \frac{6}{\sqrt[4]{3}}\sqrt{N_0}(1-S)\sqrt{\ln\frac{1}{1-S}} \tag{3.2}$$

where N_0 is the number of islands per unit surface. The fit to the distribution of the cluster perimeters extracted from the data of figure 4 requires $N_0 = 3.8 \times 10^{10}$ islands cm^{-2}. The order of magnitude of N_0 is intermediate between that of metallic clusters on metals [11] and that of diamond clusters on semiconductors [12].

It is interesting to look at the different reconstructions of the surface, changing from 7×7 of the bare Si to 5×5 of the complete Ge layer, with mixed zones at intermediate coverages. In the case of the Si(111) substrate, the 7×7 reconstruction of the clean surface is maintained up to a deposition of 0.45 ML of Ge, as confirmed by the RHEED pattern and by photoelectron diffraction [13, 14]. The absence of islands on the terraces and of reconstructed $(2 \times n)$ areas of Ge suggests a process of diffusion of Ge atoms into the Si substrate. As proposed in the case of submonolayer deposition of Ge on Si (001), Ge and Si exchange sites [15, 16] and the displaced Si diffuses towards the step edges of the substrate (displacive adsorption). Ge 2D islands appearing when the Ge coverage exceeds 1 ML have the typical

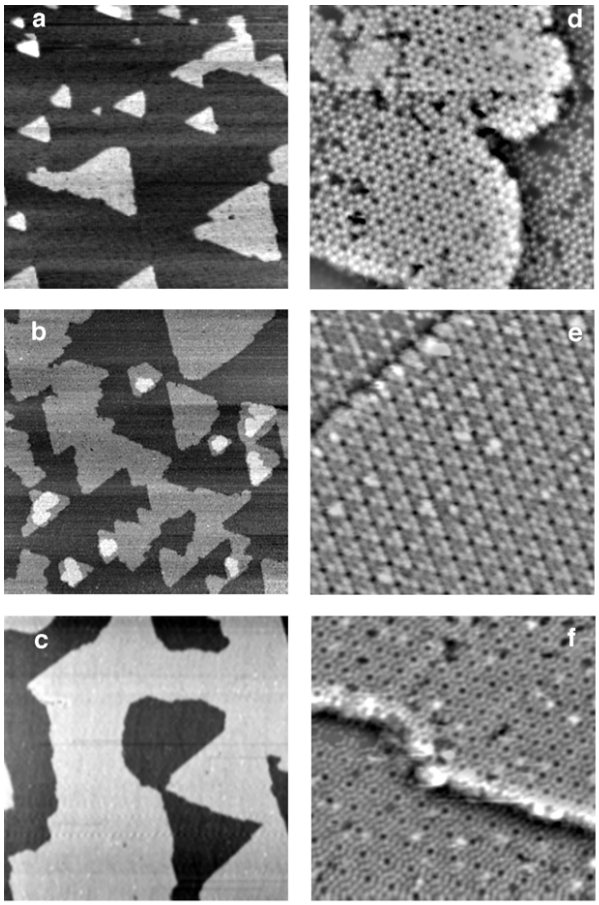

Figure 4. Left panels: evolution of the Ge/Si surface (260 × 260) nm^2 for increasing Ge thickness: (a) 0.65 ML; (b) 1.35 ML; (c) 2 ML. Right panels: corresponding enlargements (23.5 × 23.5) nm^2 of some island boundaries. Note the $(\sqrt{3} \times \sqrt{3})$R30° domain in the top left corner of panel (d) and the boundary between the 5 × 5 and 7 × 7 reconstructions (in panel (e)). The growth has been performed at $T = 500\,^{\circ}$C with a Ge flux of 0.1 nm min^{-1} [6].

5 × 5 reconstruction [17] with the inclusion of small areas with different 7 × 7 reconstruction. Such mixed phases disappear at 3 ML coverage, when the surface is flat and fully 5 × 5 reconstructed, as in figure 5.

3.2. Composition of the wetting layer

An interesting issue as regards surface composition of the 5 × 5 phase is the possibility of distinguishing Ge from Si adatoms. Some authors [18, 19] gave a positive answer to a similar question on GaAs and its ternary alloys, because the change of the tunnelling polarity makes it possible to image atoms of either electronegativity. A more refined way of obtaining the details of the wavefunction occupancy is 'current imaging tunnelling spectroscopy' (CITS), suggested for the first time by Hamers [2]. It consists of the simultaneous measurements of $I(V)$ and z at each point x, y of the surface. To obtain a CITS image, during the topographic scan at a fixed bias V_b, the feedback is disabled at each point, and the V is ramped to measure

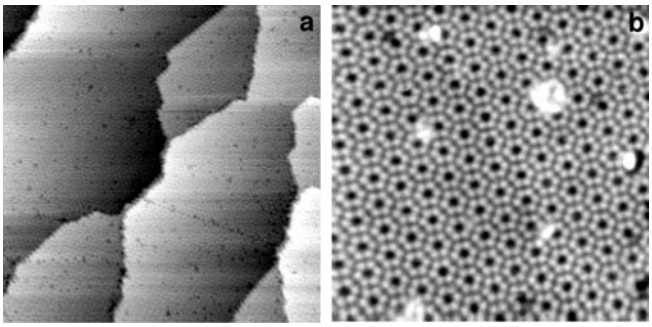

Figure 5. STM images of the Ge/Si(111) wetting layer obtained by 10 Å Ge deposition at 500 °C. (a) 150 × 150 nm. (b) 20 × 20 nm.

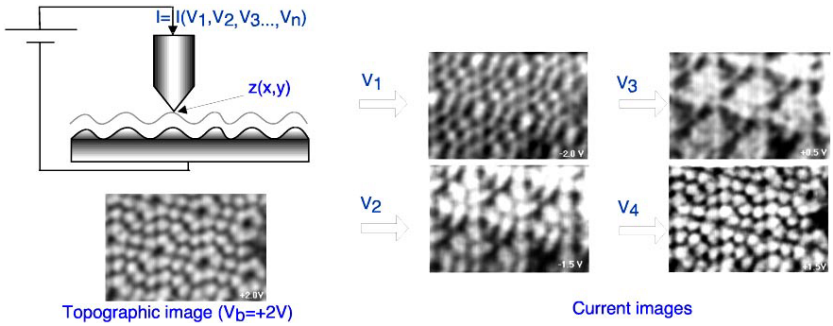

Figure 6. Current imaging tunnelling spectroscopy.

$I(V)$ (see figure 6). This solves the problem with the I–V spectroscopy caused by the thermal drift, with the result that one is never sure that the whole I–V spectrum is acquired at the same point. In CITS, data are stored as a three-dimensional matrix $I(V, x, y)$, and can be collected in current images, which are a visualization of the local electronic density at each energy. Alternatively, a different curve $I(V)$ can be extracted at each point x, y.

Unfortunately, the covalent bonding of Ge and Si does not allow for a simple distinction of the two atomic species by this technique. A first attempt was made by Becker *et al* [20] on the basis of the observed height modulation of the adatoms along selected lines of the topographic images. Later, Fukuda [7] made a statistical analysis of the height differences between neighbouring adatoms in the same half-unit and combined it with spectroscopic characterization. Within the limitations posed by the different sample preparation, the conclusions of the two authors are opposite: Becker *et al* [20] find an ordered distribution of adatoms, while Fukuda [7] suggests a random replacement of Ge atoms by Si. Very recently, Qin *et al* [21] and Sutter and Lagally [22] identified by STM the atomic sites of Ge on the Si(100) surface, assessing a random occupancy at submonolayer coverages. In order to contribute to clarifying this point, we have acquired topographic images of the 5 × 5 Ge/Si(111) surface (figure 7, panel (a)). We notice that in some of the faulted units one adatom appears darker than the other two. In several line profiles, taken on this image, we measured differences in the adatom apparent heights of each subunit of about 0.02 nm, which is comparable to the difference in covalent radii of Si (0.11 nm) and Ge (0.12 nm). This suggests either a random replacement of some Ge adatoms by Si or a bond-length relaxation caused by the presence of Si in the underlying layers. On the other hand, the Si atoms mixed in the subsurface layers could also modify the local electronic density of states on the adatoms.

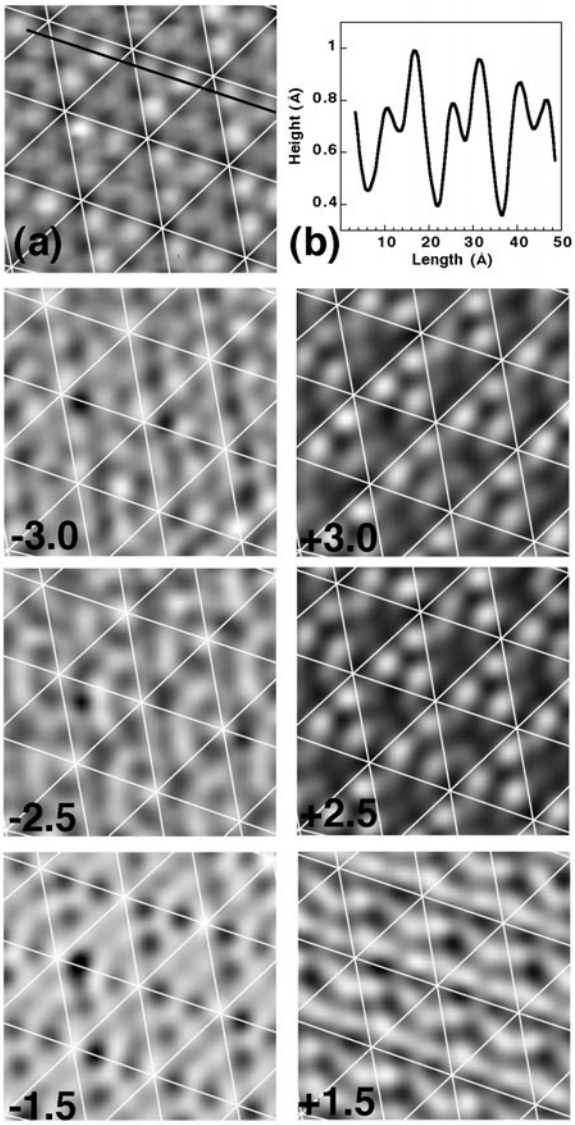

Figure 7. CITS images of the Ge/Si(111) surface after deposition of 7 ML of Ge. The image size is (4.6×4.6) nm^2. Top frame: constant-current image ($I = 1$ nA) measured with a sample bias of -2.0 V. Other frames: CITS images corresponding to: -3.0; -2.5; $-$ 1.5; +3.0; +2.5; + 1.5 V.

To analyse the electronic properties of the top layer we have collected a number of CITS spectra at different bias voltages. The data are displayed as a series of current images each for a different bias voltage. We present in figure 7 two sets of current images at 3 ML coverage, collected with negative and positive sample biases. Filled (negative-bias) and empty (positive-bias) states are imaged with atomic resolution. From the current values of the CITS images we constructed the conductance curves for those atoms, which have different brightness both in faulted and unfaulted units in the topography. For each subunit, the darker adatoms in the topography have higher conductance at positive bias; for negative bias no significant changes

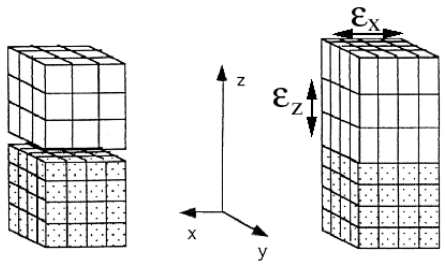

Figure 8. Tetragonal deformation of the epilayer in the heteroepitaxy.

were measured. This asymmetry could result from the fact that in the reference topography (figure 7(a)) the tip was stabilized at negative bias. The combined information drawn from topography and spectroscopy does not allow us to rule out the mixing of Ge and Si in the top-layer adatoms. To fix this point we have analysed the lattice mismatch $\varepsilon_s = (a_{\mathrm{Ge/Si}} - a_{\mathrm{Si}})/a_{\mathrm{Si}}$ as a function of coverage. We measured the lattice constant of the 5×5 unit cell by averaging the line profiles of several images acquired at the same nominal deposition. Data were collected along atomic lines as close as possible to the fast scanning direction. We find a continuous increase of ε_s up to 4% when the WL is completed (3 ML). This indicates a progressive enrichment of Ge up to about 100%. RHEED determinations of the lattice constant [23] agree satisfactorily up to 3 ML coverage with our measurements averaged over a penetration depth of 1.0 nm. We conclude that the surface layer grown at $T = 500\,^{\circ}\mathrm{C}$ is terminated with Ge atoms, in agreement with surface free-energy considerations for the Ge/Si(001) surface [24, 25]. This does not preclude random mixing of Ge and Si atoms in subsurface layers [26–28].

3.3. Evolution of a strained heterostructure

The growth of an epitaxial wetting layer is possible thanks to the tetragonal deformation of the epilayer, which elongates the lattice parameter in the perpendicular direction, in order to compensate the shrinkage in the parallel direction (figure 8). The lattice mismatch is defined as the relative difference between the lattice parameters of the two materials:

$$\text{Ge–Si } \varepsilon = \frac{d_{\mathrm{Ge}} - d_{\mathrm{Si}}}{d_{\mathrm{Ge}}} = 4\%.$$

The energy accumulated in the deformation is $E \sim k\varepsilon^2$ and it is proportional to the number of layers. The deformation is partially compensated by a tetragonal distortion. By assuming a constant volume for the distorted cell we have: $\varepsilon_z = (a_z - a_{\mathrm{Ge}})/a_{\mathrm{Ge}} = 0.08$ which gives an elongation of the lattice parameter in the z-direction $a_z = a_{\mathrm{Ge}}^{def} = 0.611$ nm. Until no dislocations appear we are in the presence of 'coherent strain'. However, for lattice mismatch like that found in Ge–Si (4%) there is a limit up to which the layer-by-layer growth is possible. This limit is usually attained at 3–5 ML, depending on the growth temperature.

Beyond this limit, the energy of the system can be lowered by the formation of 3D islands. It should be emphasized that the growth temperature influences the WL thickness both because of the different mobility of the atoms, and also by changing the composition of the epilayer because of the intermixing. This phenomenon can be analysed by EXAFS spectroscopy and will be discussed in a next section.

In a famous experiment, Jesson *et al* [29] show by AFM imaging how an initially planar 2 nm epitaxial layer of Ge/Si(001) deposited at 400 °C gives rise to 3D islands when annealed for 5 min at 600 °C. This means that if the necessary energy is available, the system can be stabilized by the formation of islands.

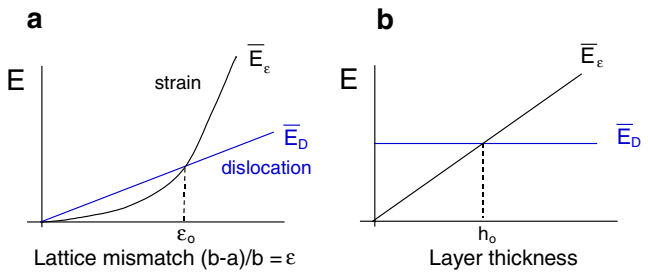

Figure 9. Energy density accumulated in the wetting layer as a function of lattice mismatch (a) and of the layer thickness (b).

3.4. Energy density accumulated in the wetting layer

It is interesting to compare the energy density accumulated in the lattice distortion versus that originating from the dislocations. Up to a certain thickness a strained layer stores less energy than a dislocated layer. In fact the distortion energy is a quadratic function of the lattice mismatch, while the number of dislocations and their energy increase linearly. Moreover the strain energy increases linearly as a function of the layer thickness, while the dislocation energy is constant (figure 9).

3.5. Nucleation of coherent islands

Coherent and strained layer-by-layer growth is favoured: for $\varepsilon < \varepsilon_0$ and for $h < h_0$. For $h > h_0$ coherent islands can nucleate. Various models have been suggested to explain the islands' nucleation mechanism. Chen and Washburn [30], following by AFM the formation of Ge/Si(001) coherent islands, suggest that 2D platelets grown over the critical size N_c become unstable, and the adatoms deposited on the wetting layer tend to diffuse and hop to the top of the platelets. So 3D islands are formed abruptly, when enough material is available.

The first discoveries of dislocation-free islands were due to Eaglesham and Cerullo [31]. They imaged by TEM islands obtained from ∼10 nm Ge deposited on Si(001) by MBE at 500 °C. In the same year Mo *et al* [32] unveiled, by STM, the detailed shape and structure of the coherent islands of Ge on Si(001). By using PVD at $T = 500\,^{\circ}\mathrm{C}$, they obtained elongated 'hut clusters', limited by lateral [501] reconstructed planes, inclined at about 10° with respect to the [001] surface. The typical height of these nanocrystals was in the range 2–5 nm, while their base was 20–40 nm. These are the most stable nanostructures of Ge/Si(001) at low coverages. Since these first discoveries many other systems have shown the formation of coherent islands. Because the island dimensions decrease by increasing the strain, by using materials such as InAs and GaAs it is indeed possible to get very small islands. The first to obtain structures under 20 nm were Oshinowo *et al* [33] who achieved 15 nm dot size in InGaAs/GaAs. Of course, larger islands can be obtained by a proper choice of the concentration x in the $In_{1-x}Ga_xAs$ alloy. Another parameter controlling the island dimension is the intermixing, which always occurs; it can be limited by using lower growth temperatures or higher growth rates [34].

3.6. Ge/Si(100): 3D island growth

A very beautiful experiment has been carried out by Voigtlaender, who succeeded in taking images of Ge islands grown on Si(001) during the nucleation and the subsequent stages [35]. The movie, which is visible at http://www.fz-juelich.de/video/voigtlaender/ shows

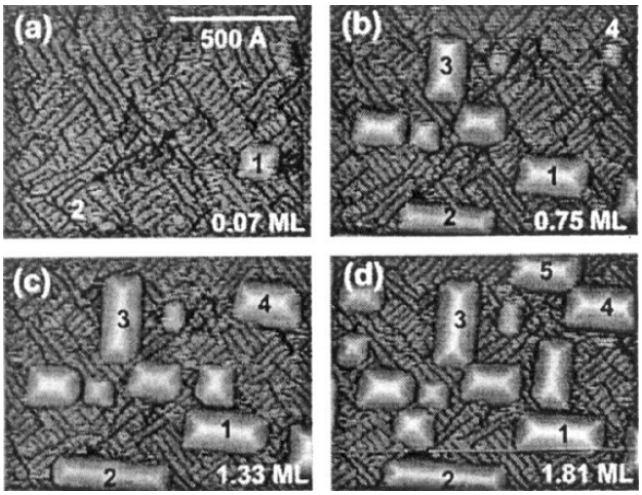

Figure 10. Evolution of hut clusters of Ge/Si(001). Courtesy of B Voigtlaender [35].

that Ge islands nucleate as square pyramids, and subsequently one side grows more rapidly than the other, giving rise to the characteristic 'hut' shape (figure 10).

This growth asymmetry can be explained with a slight fluctuation of the growth speed on one face, which completes a plane of atoms faster than the others. The subsequent planes will also be completed faster, because the perpendicular faces are now longer and need more atoms to be filled. This phenomenon is observed commonly at low growth temperatures, (300–500 °C).

Jesson *et al* [29] have explained the energy change for a square nucleus of side l on the [501] facet of a square-based pyramid. The energy needed to grow the layer is positive for small l-values, but for large l there is an energy gain due to the relaxation, which is higher towards the top of the island (figure 11). This explains the fact that there are no incomplete atomic planes, because as soon as the square nucleus overcomes the critical value, the rest of the facet is completed very fast.

At higher T (>600 °C), Medeiros-Ribeiro *et al* [36] have shown that the *most* stable structure is the square pyramid, along with its evolution (the dome), which appears when enough material is available on the surface. In his paper, Medeiros-Ribeiro fits the island distribution with two Boltzmann curves $e^{-\Delta E(n)/KT}$, which represent thermodynamic equilibrium distributions. This means that such Ge islands are stable on the Si(001) surface (which of the two shapes is favoured depends only on the number of atoms available). This does not happen on the Si(111) surface. In order to understand this phenomenon he suggests computing the free-energy difference between an island and the same amount of material spread on the wetting layer in the following form:

$$\Delta E[n] = Cn + Bn^{2/3} + An^{1/3} \ln\left[\frac{a_c}{n^{1/3}}\right]$$

where n is the number of atoms in the island (or in the wetting layer). The three terms correspond, respectively, to the bulk energy, to the surface energy, and to the edge energy. The C-coefficient (bulk energy) is negative because the atoms in the island are more relaxed than in the wetting layer; the B-coefficient (surface energy) is made of two parts: one coming from the number of dangling bonds on the surface, which is positive, and the other coming from the relaxation of the surface bonds, which is negative; the A-coefficient is positive, because of the edge energy. So the energy difference can have a minimum as a function of n.

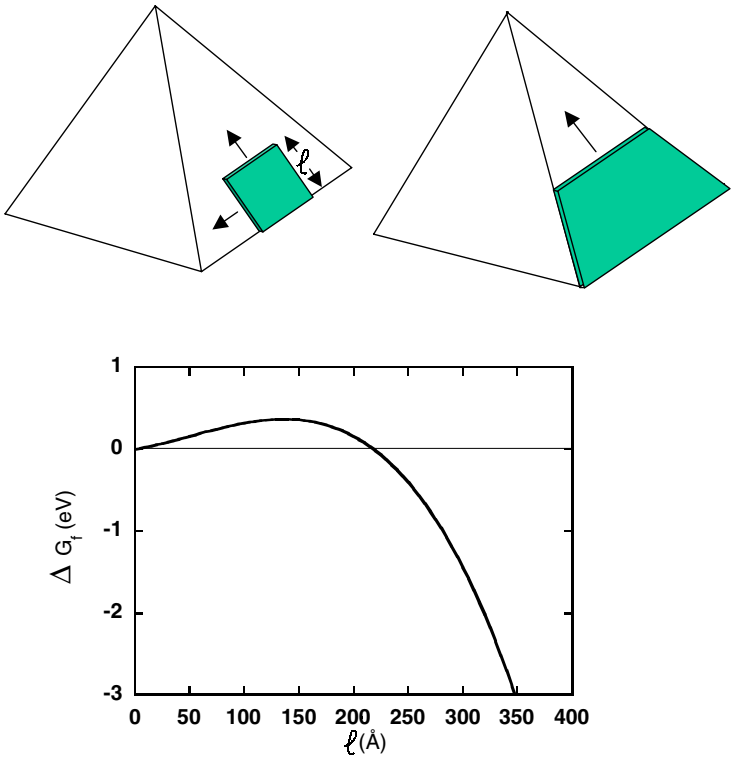

Figure 11. Energy change for a square nucleus of side l [29].

The maximum of the probability curve will correspond to this minimum. Medeiros-Ribeiro *et al* have fitted with two curves the volume distribution of Ge islands grown at 600 °C, obtaining a very good agreement with few free parameters (figure 12(B)). The transition from pyramids to domes can be explained by assuming that there are 2D Ge islands on top of the wetting layer constituting a reservoir. The nanocrystal ensemble can be considered an open system exchanging energy and atoms with 2D islands. The pyramids nucleate and grow up to a maximum volume. At this point the pyramids attract atoms from the 2D islands and the formation of a 'dome' occurs with an abrupt transition. These findings are in agreement with the theoretical predictions of Shchukin *et al* [37]. It has been also verified [38] that the island nucleation and evolution is independent of the growth method. Capellini *et al* [39, 40] and Goryll *et al* [41, 42] also report on high-and low-pressure CVD growth of Ge/Si(001) islands, confirming these data, and extending the analysis to dislocated islands. Goryll, in particular, analyses low-pressure CVD Ge/Si(001) samples, grown at $P = 0.12$ Torr and $T = 525$–700 °C (see figure 13), finding that pyramids are favoured at high deposition rate or small deposition time. The dislocated islands appear after a critical height (50 nm).

3.7. Ge/Si(100): 3D islands evolution

The evolution of Ge islands after growth during prolonged annealing has been followed by Kamins *et al*, in order to check whether the pyramids and the domes are really the most stable structures, or whether they are subject to Ostwald ripening, i.e. whether the particle size distribution coarsens, driven by the Gibbs–Thomson effect [43]. Ross *et al* [44, 45], at

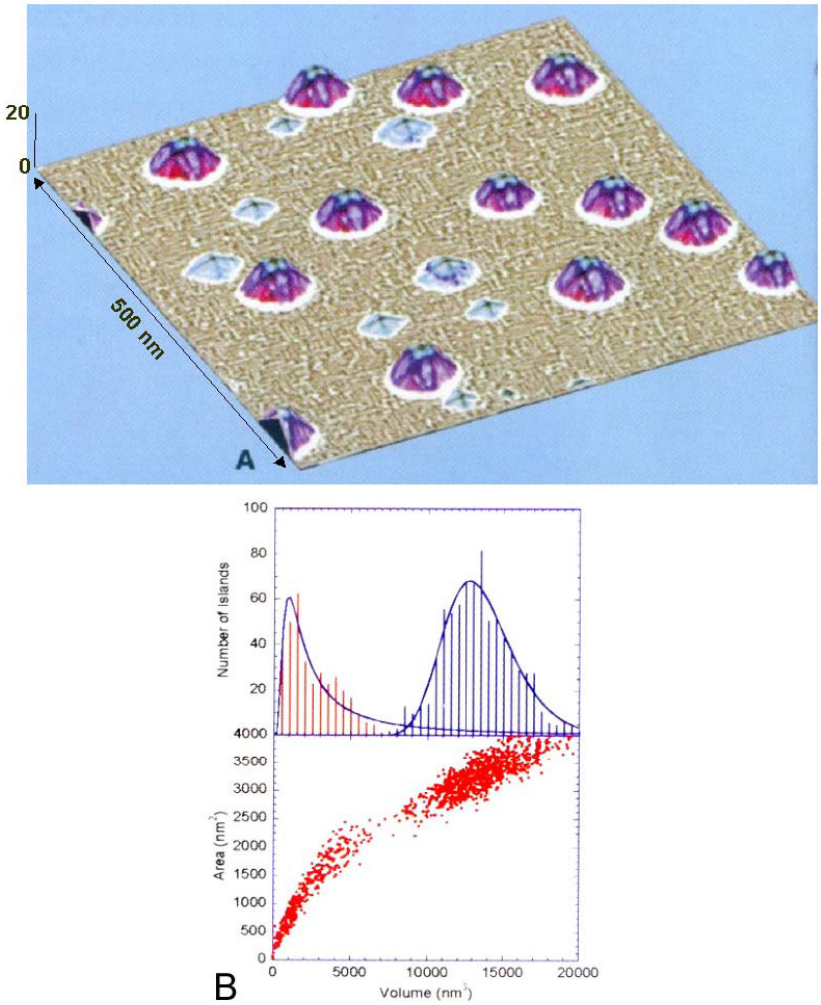

Figure 12. (A) STM topography: 10 ML Ge/Si(001) at $T = 600\,^{\circ}\mathrm{C}$. Gradient mode image: the shadings represent the local surface curvature. (B) island distributions fitted by a Boltzmann function as explained in the text. Courtesy of G Medeiros-Ribeiro [36].

high island density, found that the smaller islands shrink during annealing due to evaporation. Kamins *et al* [38] also found a ripening effect which enlarges some of the islands at the expense of the smaller ones; however, at sufficiently low temperatures the distribution is stable for the two equilibrium shapes: domes and pyramids. So Kamins *et al* state that the coarsening behaviour is not consistent with standard Ostwald ripening models [46]. The evolution of the Ge islands during the Si capping has been followed by STM at very high resolution by Rastelli *et al* [47]. They find a reversal transition from pyramid to dome with increasing Si coverage. In fact the islands transform into $\{105\}$ faceted pyramids, and eventually into stepped mounds with steps parallel to the $\langle 110 \rangle$ directions. These morphological changes are induced by alloying and represent a complete reversal of those previously observed during Ge island growth. Their results are interpreted with a simple model in which the equilibrium shape of an island mainly depends on its volume and composition.

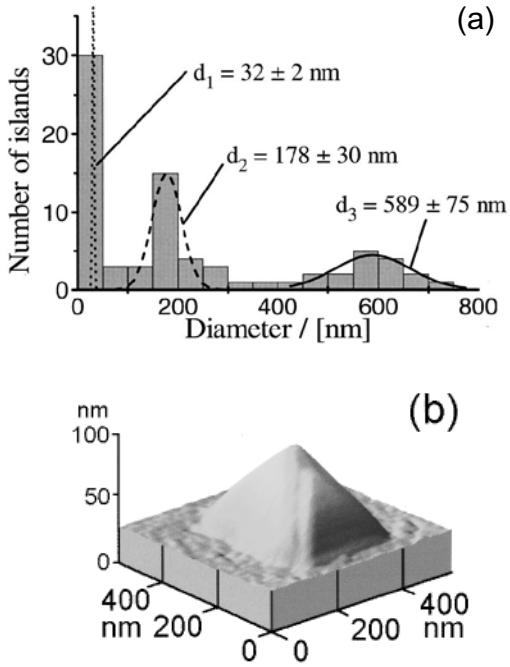

Figure 13. (a) Three-dimensional island size distribution of a Ge/Si(001) sample grown by LPCVD at 700 °C analysed by AFM. The three Gaussian size distributions were obtained by a fit to the experimental data [41]. (b) A view of a square-base pyramidal island with h 55 nm and base 300 nm (grown by CVD at 600 °C) in which a dislocation has been just inserted, forming a new growing ledge [39].

3.8. Dense array of islands

Recently, Springholz *et al* [48] and Floro *et al* [49] reported the self-organization of Ge–Si islands during growth by MBE. They have shown that generally self-limiting growth does not occur and the system is not equilibrated. Instead, self-organization occurs in a regime of high areal coverage of islands, where short-range repulsive strain interactions between islands drive the organization process. An array of hut clusters self-orders on a square mesh with increasing areal coverage. In case of a dense array of islands, Floro *et al* [50] have found that ordering occurs to minimize the repulsive elastic interactions between neighbouring islands. However, self-organization breaks down when islands coalesce during deposition or during static coarsening.

3.9. Lithographic positioning

Because self-ordering is not easy to achieve, many groups have undertaken alternative routes to auto-organization. One feasible procedure consists in the self-assembly of Ge islands on Si(001) patterned substrates. Kamins and Williams [51] have demonstrated dot positioning on Si(001) by using SiO_2 grown on Si(001). They first realized a local oxidation on the substrate defining Si lines surrounded by oxide. Epitaxial Si(001) is subsequently grown at $T = 850\,^{\circ}\mathrm{C}$ using SiH_2Cl_2 and HCl, and Ge is deposited from GeH_4 at $T = 600\,^{\circ}\mathrm{C}$ on this pattern. A similar procedure was adopted by Vescan *et al* [52], where the pattern was produced by optical lithography on SiO_2 grown on Si(001). A Si buffer layer (500 nm) is grown at $T = 800\,^{\circ}\mathrm{C}$ on

Figure 14. A schematic diagram of the formation of Ge islands on Si(111).

this patterned substrate, and the Ge is subsequently deposited at $T = 700\,^{\circ}\mathrm{C}$, 0.3 nm min^{-1} producing nice Ge dots aligned at the step edge.

4. Ge/Si(111): 3D islands

Because of its lower importance for applications, the Si(111) substrate has been rarely used for Ge growth. However, since 1991 different groups have undertaken the STM study of Ge/Si(111). First of all Köhler *et al* [53] visualized the Ge growth of the wetting layer and of the islands on Si(111). They has found that the islands are truncated pyramids, with the top 7×7 or 2×8 reconstructed, depending on the growth temperature.

In Rome Tor Vergata Laboratory, my group has recently studied *in situ* the growth of Ge/Si(111) islands. The Si substrate is prepared by flash annealing at 1250 °C through direct current heating, taking care to keep the vacuum level below 5×10^{-10} mbar during the flash. Ge is deposited by PVD from a crucible or using a low-rate electron-gun evaporator at a maximum pressure of 2×10^{-10} Torr. Si substrates are kept at 450–550 °C while the evaporation rates are typically in the range 0.2–0.5 ML min^{-1} (1 ML = 0.314 nm) as determined by a quartz thickness monitor.

3D island nucleation starts at a Ge coverage between 3 and 5 ML, depending on Ge flux and on substrate temperature (figure 14), as already noted by Kamins *et al* [38]. Typical 3D islands are shown in figure 15 where the reconstruction 5×5 of the WL and 7×7 of the tops of the islands are visible.

Initially, islands nucleate as truncated tetrahedra (figure 16), with corners pointing in the $\langle 11\bar{2} \rangle$ directions; as reported in [53], this is due to the anisotropy of the growth rate in this direction. The tops of the islands are 7×7 reconstructed (figure 15(b)), showing a substantial Ge–Si intermixing or at least a modification of the classical Ge(111) reconstruction caused by the stress fields on the island [54].

Figure 16(b), which displays the gradient of the left image, shows clearly that the island grows irrespectively of the stepping of the substrate, and that the top facet is a [111] plane. The next step in the island evolution is shown in figure 17. Now the island is much taller and new steep facets are inserted. This shape transition might be similar to that reported by Medeiros-Ribeiro *et al* [36] and Ross *et al* [44, 45], although in our case the area of the two kinds of island does not change before and after the insertion of the new facets. Notice the depression (erosion) of the substrate around the island.

The final steps of the island evolution are shown in figure 18. In panel (a) a gradient image of a Ge island at the first ripening stage is shown.

It is worth noting that the shape is rounded, and that a large amount of substrate around the island is eroded. The final ripening stage of the island is shown in panel (b); the formation of a central hole (0.6 nm deep) is the most striking feature. The overall process can be qualitatively described as follows: the islands grow vertically up to a critical height, which has been estimated to be about 48 nm [55] after which the strain energy stored inside the islands can be partially relieved by introducing dislocations, or by a morphological transition of the

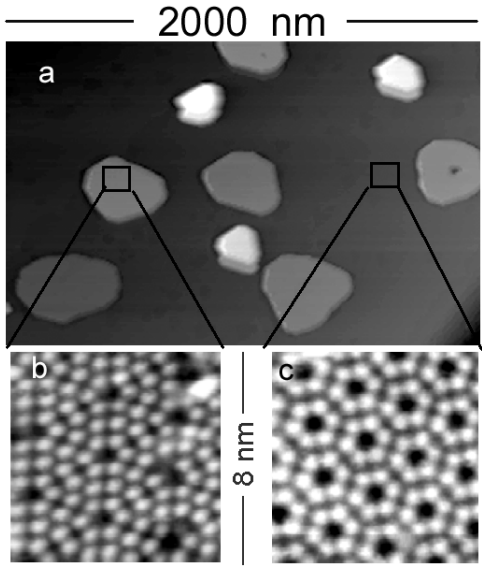

Figure 15. Topography of a Ge/Si(111) surface after deposition of 9 ML of Ge. (a) STM image, $2\times1\ \mu m^2$. Enlargements $(8 \times 8)\ nm^2$ (b) on the top of the islands and (c) on the substrate, displaying the 7×7 reconstruction of the former and the 5×5 reconstruction of the latter (from [6]).

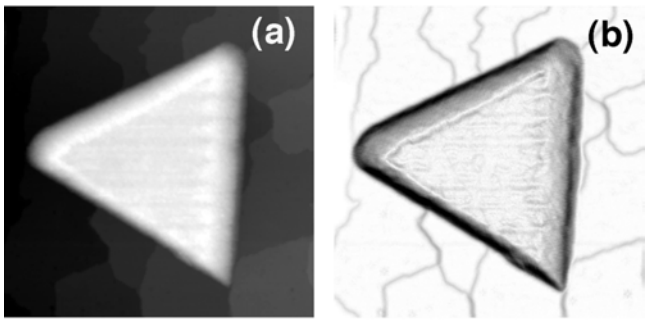

Figure 16. STM topography of a Ge island deposited on Si(111); $T = 530\,^{\circ}C$, $\theta = 2$ nm; the image dimensions are $(236 \times 236 \times 8.5)\ nm^3$. (a) Topographic image. (b) Gradient mode image. The grey levels correspond to the angles on the original images (white $= 0°$; black $= 40°$).

island which progressively becomes more rounded in shape. As regards the substrate erosion around the island, a similar effect was previously reported by Kamins *et al* [38] on Ge/Si(100); however, they could not understand its origin clearly, due to the oxidation of their samples (the measurements were performed by AFM in air) which prevented a clear imaging of the trench.

4.1. Ge–Si: erosion versus intermixing

These results lead to the idea that the erosion could be assigned to the strong Ge–Si intermixing which draws material from the substrate to create the alloy in the island. With simple geometrical analysis, Liao *et al* [56] assume that Si missing from the trenches has gone into alloying within the islands. Seifert *et al* [54] have explained the formation of trenches by using a simple model for the local strain energy density: on the WL a compressive area forms around

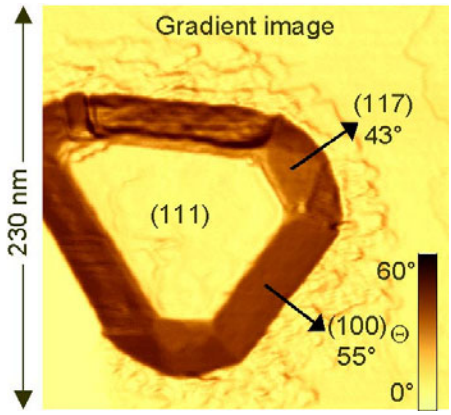

Figure 17. STM topography, imaged in gradient mode, of a Ge island deposited on Si(111) for $T = 450\,^{\circ}$C and $\theta = 2.5$ nm. The image dimensions are $(230 \times 230 \times 40)$ nm^3. The grey levels correspond to the angles on the original images (white $= 0°$; black $= 60°$).

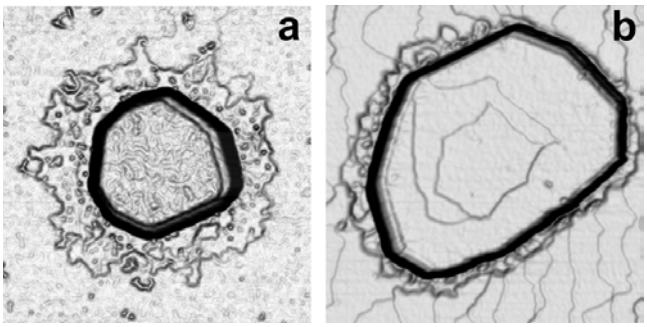

Figure 18. Ge/Si(111). (a) A 527×527 nm^2 STM image in the gradient mode of an island at the first stage of ripening. Island height: 10 nm. (b) A 527×527 nm^2 AFM image in the gradient mode of an island transformed into an atoll at the final stage. Island height: 8 nm. The two islands belong to different samples grown at $T = 530\,^{\circ}$C (3.5 and 2.0 nm of Ge/Si(111)).

an island, in which the strain energy difference (measured with respect to that of the WL far from the island) is large and positive, while inside the island it is negative [57]. This strain energy gradient is the driving force for the atom current from the WL towards the island [58], eroding the substrate that is supposed to be supercritically thick. Subsequently the island experiences a lateral growth, with material flow from the top to the edges; at the same time, the strain propagation along the substrate moves atoms from the WL to the island, eroding the WL itself and the substrate underneath. The driving force coming form the strain can explain also the erosion of the central part in the fully ripened island. We think that, according to recent calculations [59, 60], Ge atoms move towards the edge of the island's top facet, where the strain energy can be more efficiently relaxed [58]. Si atoms that come from the substrate in order to relax the strain inside the island do not have enough mobility [61] to totally replace the lacking Ge atoms, giving rise to the characteristic 'atoll' shape. We would like to point out that, remarkably, the formation of atolls is only observed for Ge grown on Si(111), and has no counterpart on the Si(001) surface.

These data confirm that in semiconductor heteroepitaxy there are basically four possible mechanisms for strain relief:

(a) island nucleation and evolution (shape transition and faceting);
(b) formation of dislocations;
(c) intermixing and alloying;
(d) formation of trenches around the islands.

In most cases, a combination of these four mechanisms takes place, and it must be emphasized that for the development of applications the formation of misfit dislocations and the occurrence of intermixing can be highly undesirable.

4.2. Ge/Si(111): Distribution of the islands on the terraces

It has been shown that during resistive heating of Si(111) a bunching of natural surface steps can occur, yielding a simple way to obtain nanostructured Si surfaces. Several authors have studied this phenomenon [62–66], demonstrating that the step configuration at a vicinal surface (with a small misorientation with respect to the (111) plane) during sublimation of a Si crystal depends on the direction of the heating current flowing through the crystal as well as on temperature. The temperature dependence of this effect is not simple, but general agreement exists on the fact that, for Si sublimation at $T > 1220\,^{\circ}$C, step bunching occurs in the step-down direction, while a regular step distribution occurs in the step-up direction. In this way we have obtained both regular (i.e. with steps naturally distributed) and step-bunched Si(111) surfaces on which we have grown epitaxially Ge at $T = 450$ and $530\,^{\circ}$C. We have analysed by STM and AFM the evolution and distribution of the islands on different surfaces. An evident self-ordering on step-bunched surfaces exists and the parameters of this ordering were studied.

Keeping the annealing temperature in the range 1220–1250 °C, and applying the voltage in the step-down direction [8], the surface reorganizes, forming large terraces (width $>1\ \mu$m) separated by groups of small steps (width ≈ 10 nm). In this case the islands start nucleating and evolving on step borders due to the Shwoebel effect. On terraces the nucleation takes place only when the step decoration is nearly completed. For 2.5 nm coverage (figures 19(a)) a line of equally spaced islands appear at the centre of the terraces, while borders are decorated by ribbons of ripened islands. They have a regular distribution, with a mean spacing of 0.39 μm and a mean distance from the steps of 0.62 μm. This gives a rough estimate ($\approx$0.5 μm) of the diffusion length of Ge on these surfaces. At 6 nm (figure 19(b)) several generations of islands are present on the terraces, from the youngest (tall and triangular) to the oldest (rounded, atoll-like), while step edges are covered by a continuous ribbon. It is very interesting to observe that a regular distribution of islands has been obtained by CVD growth on lithographically patterned substrates by Kamins and Williams [51] and by Vescan *et al* [52]. Our experiments show that in principle the same is possible on Si(111), just by using the natural patterning due to step bunching.

On applying the voltage in the step-up direction during annealing at $T = 1220\,^{\circ}$C, steps distribute uniformly (step width $\approx$70 nm). On this regular substrate, islands nucleate without any specific ordering (figures 19(c), (d)) except for a tendency of the islands to align in the direction parallel to the step borders. It is also notable that tetrahedral islands point in the same $\langle 11\bar{2}\rangle$ direction both on step-bunched and on regular surfaces.

4.3. Ge/Si(111): effects of annealing

In order to analyse the effect of annealing on Ge islands, we have grown two different samples at 500 °C by depositing 4 nm Ge on Si(111) at 0.05 nm min^{-1}. The two samples were annealed at 500 °C just after the growth for 5 min (figure 20(a)) and 30 min (figure 20(b)).

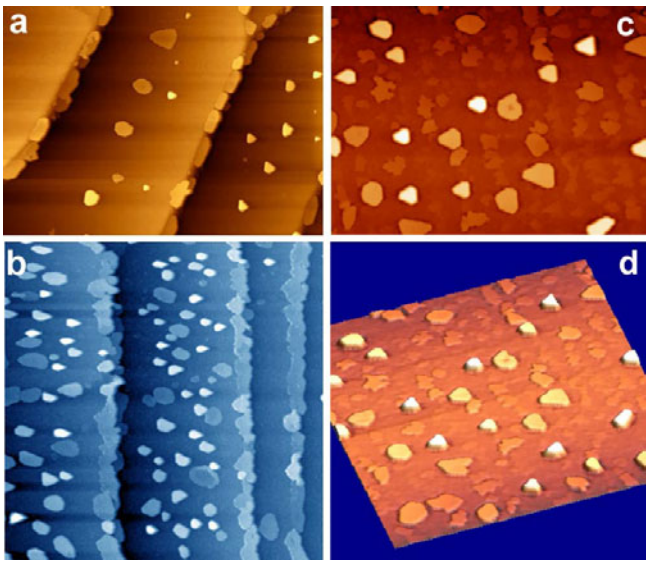

Figure 19. (a) An STM image of 2.5 nm Ge deposition on Si(111) at $T = 450\,^{\circ}\mathrm{C}$ $2.7 \times 2.7\ \mu\mathrm{m}^2$. The total height of the image is 56 nm. (b) An STM image of 6 nm Ge deposition on Si(111) at $T = 450\,^{\circ}\mathrm{C}$ $10 \times 10\ \mu\mathrm{m}^2$. The total height of the image is 82 nm. (c) 5.4 nm Ge deposited at $T = 500\,^{\circ}\mathrm{C}$ on a regular surface: $(3 \times 3)\ \mu\mathrm{m}^2$; vertical scale: 29 nm. (d) A 3D representation of image (c). The Si(111) substrate has been flashed at $T = 1200\,^{\circ}\mathrm{C}$.

In figure 21(a) we report the height distribution of the island sizes of the above-mentioned samples obtained by performing measurements on about 200 islands. In the curve of the 5 min annealed sample we recognize a peak A centred around 48 nm and a broad structure B centred around 20 nm. In the 30 min annealed sample we observe a narrowing of the B band to just one peak, and a shift of structures A and B toward lower height. This means that the islands are not stable against annealing, and there is a tendency to relax the stress by moving atoms from the island top to the island base. The introduction of Misfit Dislocations (MDs) surely plays a role in this transition, by changing the island shape from truncated tetrahedra to flat discs, up to the last stage of atolls.

Comparing the effects seen during annealing with those observed during growth we are able to consider the evolution of 3D islands. On increasing Ge coverage, the islands grow via a SK self-assembling mechanism as truncated tetrahedra until they reach a height of 48–50 nm. In agreement with the Ge/Si(100) case [39], we take this value as the critical height for the introduction of MDs. In fact it has been reported that when the strain energy stored in the island is too high, MDs are inserted in the [110] direction [67].

The regions where an MD has been inserted are stress free and thus are preferential sites for Ge attachment [39, 57]. In our case we suggest that this mechanism drives the morphological evolution of the islands from coherent to dislocated during annealing. During the annealing procedure we can observe the evolution of this relaxation over time, keeping the number of Ge atoms deposited fixed. As during growth, the atoms that are bonded in the top of a strained island experience a stress that decreases the energy barrier for detachment [68]. In contrast, the sites where stress has been induced have a higher binding energy: this difference in the energy gained by the system bonding an atom (i.e. an inhomogeneous chemical potential) generates a flow of atoms [69] that depletes the top of the island and increases the material deposited at its base. In that way we can have a 'damping' of the island that increases the dimension of the top facet and decreases the contact angle of the facets in a way that agrees with our observations.

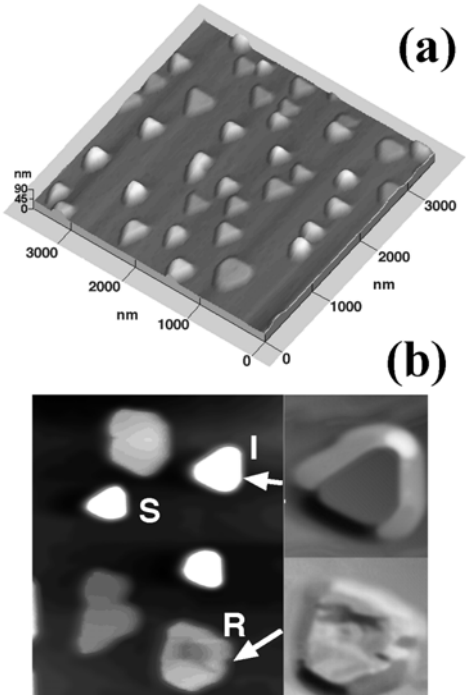

Figure 20. (a) A 4×4 μm^2 AFM image of 4 nm Ge deposition with annealing for 5 min at $T = 500\,^{\circ}$C; (b) a 2×2 μm^2 AFM image of 4 nm Ge deposition with annealing for 30 min at $T = 500\,^{\circ}$C. The total height of the image is 45 nm. The three labels stand for strained, intermediate, and relaxed. Notice the rounding of the corner of the island I due to the introduction of MDs and the atoll-like shape of island R (from [55]).

4.4. Ge/Si(111): intermixing measured by XAFS

By using x-ray absorption fine structure at the Ge K edge in fluorescence mode [70, 71], Boscherini *et al* have provided direct evidence of Si–Ge intermixing in self-organized strained and unstrained Ge QDs on Si, and a quantitative measurement of the average composition for different growth conditions. For Ge/Si(001) dots with equivalent thickness in the range 5.8–38 nm and morphology ranging from that typical of coherently strained to that associated with relaxed dots we have found that the average Si concentration is ≈30%. For Ge/Si(111) (measured in the range 1.7–6 nm), we have found that both the wetting layer and islands have a Si concentration near 50% [72].

In figure 22 the number of Si atoms around Ge, obtained from the fit of the Ge/Si(111) XAFS spectra, is shown as a function of deposited Ge thickness. The data refer to substrate temperatures of 450 ± 20 and $530 \pm 20\,^{\circ}$C. The number of Si atoms decreases from 2 to 1 with increasing thickness. This means that intermixing decreases from 50% (as previously reported [70–72]) to 25%. Moreover, samples grown at higher T display higher values of n, which points to a larger intermixing. Interesting experiments on this aspect have been performed by Capellini *et al* [73], who analysed by XPS the Si content in Ge/Si(001) islands grown at different temperatures by CVD, finding an increase of intermixing in the islands at higher temperatures. Our intermixing (ranging from about 25% for samples with 3D islands to 50% for samples with WL only), matches well the observed lateral size of the islands (up to 200–300 nm). In fact this size is considerably larger than that measured on typical Ge/Si islands

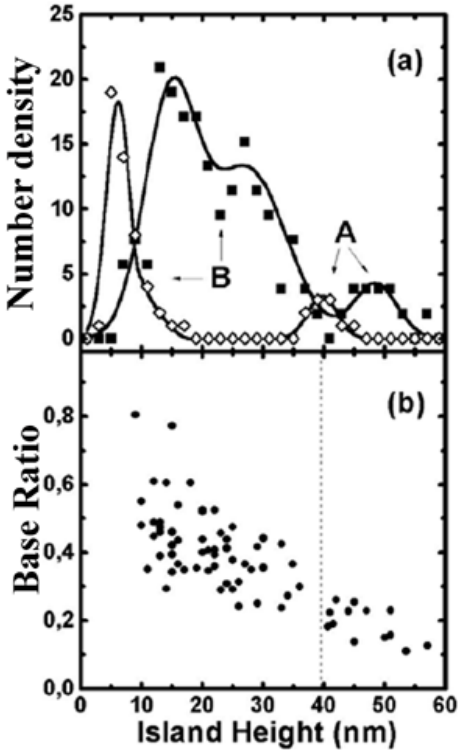

Figure 21. (a) Island height distributions of the 5 min (square) and 30 min annealed (diamond) sample displayed in figure 31. (b) The ratio R between the top and bottom base sizes of the islands in the 5 min annealed sample. The vertical dashed line separates the A-type from the B-type islands (from [31]).

(40–80 nm) grown by fast evaporation or by CVD [39, 74]. The decrease of intermixing with thickness, shown in figure 22, is connected to the increase of Ge in the 3D islands at the expense of the WL. We suggest that Si content is limited both by diffusion (the height of the islands can reach 50 nm) and from the fact that in the islands the lattice is more relaxed than in the WL, thereby reducing the driving force for intermixing. The interdiffusion mechanism of Ge/Si interface has been extensively discussed in a recent paper by Brunner [75], concluding that Ge segregation in Si is energetically favourable, but that it depends critically on the temperature. At temperatures $>450\,^{\circ}$C, a thermal equilibrium state of segregation is reached, and a segregation length of several nanometres is attained. Following Brunner, interdiffusion of Si and Ge at buried Si/SiGe heterointerfaces is described by Fick's law, $D(T) = D_0 \exp(-E_a/k_B T)$ with a diffusion constant D_0 depending on temperature, Ge content, and lattice strain. The constant D_0 is about 0.2 cm^2 s^{-1} for Si/Ge intermixing. The thermal activation energy E_a depends on Ge content and is smaller (3.1 eV) for Ge concentration $x > 0.3$ and larger (4.7 eV) for low Ge content. At a given substrate temperature, the resulting different diffusion constants within the Si host and the Ge-rich layer or nanostructure cause concentration profiles that are smeared out very asymmetrically: Ge-rich regions rapidly intermix with Si and a rather homogeneous lowering of the Ge content is expected in the whole Ge-rich layer. In a recent paper Liao *et al* [76] report a detailed EDX analysis of the concentration profile of Ge/Si(100) islands, showing that the Si/Ge intensity ratio reaches 1.5 at the base of the island, and decreases to 0.5 at the

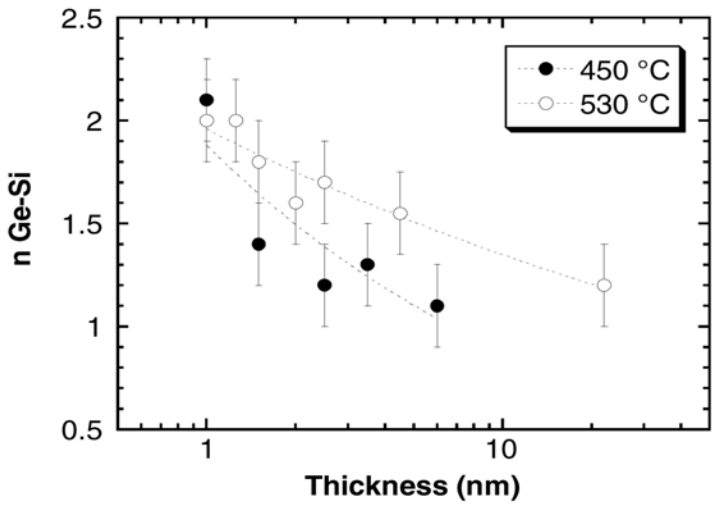

Figure 22. The average number of Si atoms around a Ge absorber obtained by fitting XAFS data taken on Ge/Si(111) samples grown at 450 and 530 °C substrate temperature [72].

top. This result is not quantitative, because the X-signal ratio has not been translated into a Si/Ge composition ratio, but it is in substantial agreement both with the suggestion of Brunner and with our XAFS results.

5. Conclusions

We have shown how the new SPM techniques can give a lot of information on the growth and morphology of semiconductor QDs. We have analysed the origin of QD formation, which is connected to the strain coming from the difference in lattice parameter between the substrate and the epilayer. At a critical layer thickness, the growth mode changes from 2D to 3D and small islands appear. We have analysed in detail the growth of QDs in a prototypical system: Ge/Si. This could be regarded as a model SK system, but intermixing between Ge and Si is very important especially at high temperatures, often limiting the minimum dot size to more than 100 nm. We analysed first the evolution and the composition of the wetting layer and then the nucleation and the formation of coherent 3D islands. On Si(100) substrates the QDs nucleate as square-based pyramids, evolving into domes which are the most stable structures. Dislocated islands appear after a certain size, if Ge deposition is continued. The final evolution of the islands depends on the subsequent thermal treatment, and eventually dislocated and ripened islands are produced. On Si(111) substrates, islands nucleate as truncated tetrahedra, adding new facets as the size increases. As Si(111) is a minimum-energy surface, the islands tend to flatten and to enlarge the top (111) face. Many dislocations are introduced, and the final shape resembles an 'atoll' due to the erosion of the central part of the island. This erosion is supposed to be caused by a tensile stress found by the atoms in this region, due to the particular composition profile.

We have discussed the stability and the possible routes for organizing QDs, notably self-ordering caused by repulsive strain fields on Si(100), or by step-bunched surfaces on Si(111).

Finally, we studied by XAFS the problem of intermixing between Ge and Si, determining the average composition of the wetting layer and of the islands.

The possible applications of Ge/Si QDs are various, but only the creation of nanomemories

seems actually to have a viable solution. The optical properties of these materials are quite limited because of the indirect Si gap, and the emission can reach appreciable values only at low T. There is still a lot of work to be done in this field, in order to find the way to generate ordered arrays of perfect QD structures. Many solutions have been suggested combining standard lithography and self-assembling (see for example [77]). Also the problem of contacting these structures has not yet been solved. It is actually not known whether the miniaturization of future electronics will be reached by self-assembled QDs, producing 'nanoelectronics', i.e. if these structures can really be grown in an organized way at the desired size. Moreover, their interconnection is still very difficult, and no one can say when the creation of nanomemories will be achievable. The answers are left to the many researchers faced every day with new challenges in controlling the growth of these structures.

Acknowledgments

I am deeply indebted to all the scientists who contributed substantially to these studies. Special thanks go to Dr A Sgarlata for all the work done with me on Ge/Si(111) and particularly for the acquisition of the Ge/Si movies. Thanks are due to Dr F Rosei, who produced many of the images shown in this paper in the framework of his PhD Thesis. Dr R Calarco, Dr M Scarselli, Dr S Nufris, and Dr E Placidi are also gratefully acknowledged for their work on STM and AFM of Ge/Si. I would like to thank also Professor M De Crescenzi, Professor M Fanfoni, Professor F Patella, Professor F Boscherini, and Dr G Capellini for fruitful collaboration at various stages of Ge–Si research. I am especially indebted to Professor A Balzarotti for his continuous and stimulating support of all this work. Finally I would like to thank the INFM (Istituto Nazionale di Fisica della Materia) which financed the VT-STM microscope in the framework of 'Large Instruments Funding' and all the people at the Physics Department of the University of Rome Tor Vergata, where I worked for the last 15 years, and where all the STM measurements shown in this paper were obtained.

References

[1] Binning G and Rohrer H 1999 *Rev. Mod. Phys.* **71** S324
Kubby J A and Boland J J 1996 *Surf. Sci. Rep.* **26** n3–6
Wiesendanger R 1994 *Scanning Probe Microscopy and Spectroscopy: Methods and Applications* (Cambridge: Cambridge University press)
[2] Hamers R J 1989 *Annu. Rev. Phys. Chem.* **40** 531 and references therein
[3] Voigtlaender B and Zinner A 1993 *Appl. Phys. Lett.* **63** 3055
Voigtländer B, Zinner A and Weber Th 1996 *Rev. Sci. Instrum.* **67** 2568
Voigtländer B 2001 *Surf. Sci. Rep.* **43** 127
[4] Marchi F, Bouchiat V, Dallaporta H, Safarov V, Tonneau D and Doppelt P 1998 *J. Vac. Sci. Technol.* B **16** 2952
[5] Kohmoto S, Nakamura H, Ishikawa T and Asakawa K 1999 *Appl. Phys. Lett.* **75** 3488
[6] Motta N, Sgarlata A, Calarco R, Nguyen Q, Patella F, Castro Cal J, Balzarotti A and De Crescenzi M 1998 *Surf. Sci.* **406** 254
Rosei F, Motta N, Sgarlata A, Capellini G and Boscherini F 2000 *Thin Solid Films* **369** 29
Arciprete F, Balzarotti A, Fanfoni M, Motta N, Patella F and Sgarlata A 2001 *Recent Res. Devel. Vac. Sci. Technol.* **3** 71
[7] Fukuda T 1996 *Surf. Sci.* **351** 103
[8] Motta N, Sgarlata A, Rosei F and Balzarotti A 2002 *Mater. Res. Symp. Proc.* **696** N2.2.1
[9] Avrami M 1939 *J. Chem. Phys.* **7** 1103
Avrami M 1940 *J. Chem. Phys.* **8** 212
[10] Tomellini M and Fanfoni M 1996 *Surf. Sci.* **349** L191
[11] Brune H, Roder H, Boragno C and Kern K 1994 *Phys. Rev. Lett.* **73** 1955
[12] Polini R, Tomellini M, Fanfoni M and Le Normand F 1997 *Surf. Sci.* **373** 230

[13] Lamin M A, Pchelyakov O P, Sokolov L V, Stenin S I and Toropov A I 1989 *Surf. Sci.* **207** 418
[14] De Crescenzi M, Gunnella R, Bernardini R, De Marco M and Davoli I 1995 *Phys. Rev.* B **52** 1806
[15] Tromp R M 1993 *Phys. Rev.* B **47** 7125
Patthey L, Bullock E L, Abukawa T, Kono S and Johansson L S O 1995 *Phys. Rev. Lett.* **75** 2538
[16] Huang K H, Ku T S and Lin D S 1997 *Phys. Rev.* B **56** 4878
[17] Köhler U, Jusko O, Pietsch G, Muller B and Henzler M 1991 *Surf. Sci.* **248** 321
[18] Feenstra R M, Stroscio J A, Tersoff J and Fein A P 1987 *Phys. Rev.* **58** 192
Feenstra R M 1989 *Phys. Rev. Lett.* **63** 1412
[19] Salemink H W M and Albrektsen O 1993 *Phys. Rev.* B **47** 16 044
[20] Becker R S, Golovchenko J A and Swartzentruber B S 1985 *Phys. Rev.* B **32** 8455
[21] Qin X R, Swartzentruber B S and Lagally M G 2000 *Phys. Rev. Lett.* **84** 4645
[22] Sutter P and Lagally M G 2000 *Phys. Rev. Lett.* **84** 4637
[23] Deelman P W, Thundat T and Schowalter L J 1996 *Appl. Surf. Sci.* **104–5** 510
[24] Liu F and Lagally M G 1996 *Phys. Rev. Lett.* **76** 3156
[25] Liu F and Lagally M G 1997 *Chem. Rev.* **97** 1045
[26] Kelires P C and Tersoff J 1989 *Phys. Rev. Lett.* **63** 1166
[27] Jesson D E, Pennycook S J and Baribeau J M 1991 *Phys. Rev. Lett.* **66** 750
[28] Jesson D E, Chrisholm M F, Pennycook S J and Baribeau J M 1995 *Phys. Rev. Lett.* **75** 184
[29] Jesson D E, Chen K M and Pennycook S J 1996 *MRS Bull.* **21** 31
[30] Chen Y and Washburn J 1996 *Phys. Rev. Lett.* **77** 4046
[31] Eaglesham D J and Cerullo M 1990 *Phys. Rev. Lett.* **64** 1943
[32] Mo Y-W, Savage D E, Swartzentruber B S and Lagally M G 1990 *Phys. Rev. Lett.* **65** 1020
[33] Oshinowo *et al* 1994 *Appl. Phys. Lett.* **65** 1422
[34] Patella F, Fanfoni M, Arciprete F, Nufris S, Placidi E and Balzarotti A 2001 *Appl. Phys. Lett.* **78** 320
[35] Kastner M and Voigtlaender B 1999 *Phys. Rev. Lett.* **82** 2745
[36] Medeiros-Ribeiro G, Bratkovski A M, Kamins T I, Ohlberg D A and Williams R S 1998 *Science* **279** 353
[37] Shchukin V A, Ledentsov N N, Kop'ev1 P S and Bimberg D 1995 *Phys. Rev. Lett.* **75** 2968
[38] Kamins T I, Medeiros-Ribeiro G, Ohlberg D A A and Williams R S 1999 *J. Appl. Phys.* **85** 1159
[39] Capellini G, Di Gaspare L, Evangelisti F and Palange E 1997 *Appl. Phys. Lett.* **70** 493
Capellini G, Di Gaspare L, Evangelisti F and Palange E 1999 *Semicond. Sci. Technol.* **14** L21
[40] Palange E, Capellini G, Di Gaspare L and Evangelisti F 1996 *Appl. Phys. Lett.* **68** 2982
Palange E, Ragni L, Di Gaspare L, Capellini G and Evangelisti F 1998 *J. Appl. Phys.* **83** 5840
[41] Goryll M, Vescan L, Schmidt K, Mesters S, Luth H and Szot K 1997 *Appl. Phys. Lett.* **71** 410
[42] Goryll M, Vescan L, Schmidt K, Mesters S, Luth H and Szot K 2000 *Mater. Sci. Eng.* B **69–70** 251
[43] Ostwald W 1900 *Z. Phys. Chem.* **34** 495
[44] Ross F M, Tromp R M and Reuter M C 1999 *Science* **286** 193
[45] Ross F M, Tersoff J and Tromp R M 1998 *Phys. Rev. Lett.* **80** 984
[46] Zinke-Allmang M, Feldman L C and Grabow M H 1992 *Surf. Sci. Rep.* **16** 377
[47] Rastelli A, Kummer M and von Kanel H 2001 *Phys. Rev. Lett.* **87** 256101
Rastelli A, Muller E and von Kanel H 2002 *Appl. Phys. Lett.* **80** 1438
[48] Springholz G, Holy V, Pinczolits M and Bauer G 1998 *Science* **282** 734
[49] Floro J A, Chason E, Sinclair M B, Freund L B and Lucadamo G A 1998 *Appl. Phys. Lett.* **73** 951
[50] Floro J A, Sinclair M B, Chason E, Freund L B, Twesten R D, Hwang R Q and Lucadamo G A 2000 *Phys. Rev. Lett.* **84** 701
[51] Kamins T I and Williams R S 1997 *Appl. Phys. Lett.* **71** 1201
[52] Vescan L, Grimm K, Goryll M and Hollander B 2000 *Mater. Sci. Eng.* B **69** 324
[53] Köhler U, Jusko O, Pietsch G, Muller B and Henzler M 1991 *Surf. Sci.* **248** 321
[54] Seifert W, Carlsson N, Johansson J, Pistol M and Samuelson L 1977 *J. Cryst. Growth* **170** 39
[55] Capellini G, Motta N, Sgarlata A and Calarco R 1999 *Solid State Commun.* **112** 145
[56] Liao X Z, Zou J, Cockayne D J H, Jiang Z M, Wang X and Leon R 2000 *Appl. Phys. Lett.* **77** 1304
[57] Le Goues F K, Reuter M C, Tersoff J, Hammar M and Tromp R M 1994 *Phys. Rev. Lett.* **73** 300
[58] Barabási A-L 1997 *Appl. Phys. Lett.* **70** 2565
Chaparro S A, Zhang Y and Drucker J 2000 *Appl. Phys. Lett.* **76** 3534
[59] Tersoff J 1998 *Phys. Rev. Lett.* **81** 3183
[60] Spencer B J and Tersoff J 2001 *Phys. Rev.* B **63** 205424-1
[61] Tersoff J 2000 *Phys. Rev. Lett.* **85** 2843
[62] Metois J J and Stoyanov S 1999 *Surf. Sci.* **440** 407
[63] Homma Y and Aizawa N 2000 *Phys. Rev.* B **62** 8323

[64] Jeong H-C and Williams E D 1999 *Surf. Sci. Rep.* **34** 171–294
[65] Yagi K, Minoda H and Degawa M 2001 *Surf. Sci. Rep.* **43** 45–126
[66] Men F K, Liu F, Wang P J, Chen C H, Cheng D L, Lin J L and Himpsel F J 2002 *Phys. Rev. Lett.* **88** 096105
[67] Le Goues F K, Reuter M C, Hammar M and Tromp R M 1996 *Surf. Sci.* **349** 249
[68] Dobbs H T, Vvedensky D D, Zangwill A, Johansson J, Carlsson N and Seifert W 1997 *Phys. Rev. Lett.* **79** 897
[69] De Crescenzi M, Gunnella R, Bernardini R, De Marco M and Davoli I 1995 *Phys. Rev.* B **52** 1806
[70] Boscherini F, Capellini G, Di Gaspare L, Rosei F, Motta N and Mobilio S 2000 *Appl. Phys. Lett.* **76** 682
[71] Boscherini F, Capellini G, Di Gaspare L, De Seta M, Rosei F, Sgarlata A, Motta N and Mobilio S 2000 *Thin Solid Films* **380** 173
[72] Motta N, Boscherini F, Capellini G, Rosei F, Sgarlata A and Mobilio S 2002 *Mater. Sci. Eng.* B **88** 264
[73] Capellini G, De Seta M and Evangelisti F 2001 *Appl. Phys. Lett.* **78** 303
[74] Kajiyama H *et al* 1992 *Phys. Rev.* B **45** 14 005
[75] Brunner K 2002 *Rep. Prog. Phys.* **65** 27–72
[76] Liao X Z, Zou J, Cockayne D J H, Jiang Z M, Wang X and Leon R 2000 *Appl. Phys. Lett.* **77** 1304
[77] Omi H, Bottomley D J and Ogino T 2002 *Appl. Phys. Lett.* **80** 1073